The Astronomical Journal, 134:1662–1670, 2007 October

COOL CUSTOMERS IN THE STELLAR GRAVEYARD. IV. *SPITZER* SEARCH FOR MID-IR EXCESSES AROUND FIVE DAs[1]

John H. Debes,[2] Steinn Sigurdsson,[3] and Brad Hansen[4]

Received 2007 February 28; accepted 2007 June 27

ABSTRACT

Hydrogen atmosphere white dwarfs with metal lines, so-called DAZs, require external accretion of material to explain the presence of weak metal-line absorption in their photospheres. The source of this material is currently unknown, but could come from the interstellar medium, unseen companions, or relic planetesimals from asteroid belt or Kuiper Belt analogs. Accurate mid-infrared photometry of these white dwarfs provides additional information to solve the mystery of this accretion and to look for evidence of planetary systems that have survived post-main-sequence evolution. We present *Spitzer Space Telescope* IRAC photometry accurate to ~3% for four DAZs and one DA with circumstellar absorption lines in the UV. We search for excesses due to unseen companions or circumstellar dust disks. We use *Hubble Space Telescope* NICMOS imaging of these white dwarfs to gauge the level of background contamination to our targets, as well as to rule out common proper motion companions to WD 1620−391. All of our targets show no excesses due to companions >20 M_J, ruling out all but very low mass companions to these white dwarfs at all separations. No excesses due to circumstellar disks are observed, and we place limits on what types of disks may still be present.

Key words: circumstellar matter — planetary systems — white dwarfs

Online material: color figures

1. INTRODUCTION

White dwarfs have long been used to probe the low-mass end of the initial mass function to look for low-mass stellar and brown dwarf companions (Probst & O'Connell 1982; Zuckerman & Becklin 1992; Farihi et al. 2005). With the advent of more sensitive ground- and space-based imaging at longer wavelengths, the direct detection of substellar objects and planets with a few times Jupiter's mass around white dwarfs is now possible (Ignace 2001; Burleigh et al. 2002; Friedrich et al. 2005; Farihi et al. 2005; Debes et al. 2005a, 2005b).

Searching a subset of white dwarfs that harbor markers for substellar objects can maximize the return of such a survey. Nearby hydrogen white dwarfs with metal-line absorption (DAZs) may fit this criterion. Three hypotheses have been put forth to explain the presence of DAZs: interstellar matter (ISM) accretion (Dupuis et al. 1992,1993a,1993b; Koester & Wilken 2006), unseen companion wind accretion (Zuckerman et al. 2003), and accretion of volatile poor planetesimals (Alcock et al. 1986; Debes & Sigurdsson 2002; Jura 2003).

ISM accretion has a wealth of problems in predicting many aspects of DAZs, such as the large accretion rates required for some objects and the distribution of these objects with respect to known clouds of dense material (Aannestad et al. 1993; Zuckerman & Reid 1998; Zuckerman et al. 2003; Kilic & Redfield 2007). The quick atmospheric settling times of hydrogen atmospheres imply that the white dwarfs are in close proximity to accretionary material.

There are roughly 40 cool DAZs known (Zuckerman et al. 2003; Koester & Wilken 2006). Of them, seven have dM companions, supporting the argument that DAZs could have unseen companions that place material onto the WD surface through winds (Zuckerman et al. 2003; Debes 2006). In order to accrete enough material, companions must be in extremely close orbits ($P \lesssim 1$ day), bringing into question why these objects have yet to be discovered through radial velocity surveys of compact objects or observable excesses in near-IR flux. In most cases the reflex motion from such objects would be easily detectable, on the order of a few to tens of km s^{-1} (Zuckerman & Becklin 1992; Maxted et al. 2006). The presence of unseen companions also cannot explain objects like G29-38 and four other white dwarfs which have infrared excesses due to dust disks within their host white dwarf's tidal disruption radius (Graham et al. 1990; Patterson et al. 1991; Jura 2003; Becklin et al. 2005; Reach et al. 2005b; Kilic et al. 2006a). The disks around G29-38 and GD 362 show an amorphous silicate emission feature at ~10 μm, implying a small grain size within the disk and possibly warped geometries (Reach et al. 2005b; Jura et al. 2007b). Furthermore, companions >13 M_J are ruled out for a wide range of orbital separations around G29-38 (Debes et al. 2005a).

The invocation of cometary or asteroidal material as a method of polluting WD atmospheres was developed to explain photospheric absorption lines due to metals in the DAZ WD 0208+395 (G74-7; Alcock et al. 1986). However, the rates predicted by these original studies could not satisfactorily explain the highest accretion rates inferred for some objects and could not easily reproduce the distribution of DAZs based on their effective temperatures (Zuckerman et al. 2003). Mixing length theory, however, predicts a drop-off of observability for accretion as a function of effective temperature which may swamp out the earlier prediction of Alcock et al. (1986) (Althaus & Benvenuto 1998). Also unclear is the effect nonaxisymmetric mass loss could have on the fraction of comet clouds lost by their hosts during post-main-sequence evolution (Parriott & Alcock 1998). By hypothesis, cometary

[1] Based in part on observations made with the NASA/ESA *Hubble Space Telescope*, obtained at the Space Telescope Science Institute, which is operated by the Association of Universities for Research in Astronomy, Inc., under NASA contract NAS 5-26555. These observations are associated with program 10560.

[2] Department of Terrestrial Magnetism, Carnegie Institution of Washington, Washington, DC 20015, USA.

[3] Department of Astronomy and Astrophysics, Pennsylvania State University, University Park, PA 16802, USA.

[4] Department of Astronomy, UCLA, Los Angeles, CA 91125, USA.

TABLE 1
PROPERTIES OF THE TARGET WHITE DWARFS

WD	Name	M_f ($M_\odot$)	$T_{\rm eff}$ (K)	$t_{\rm cool}$ (Gyr)	D (pc)	M_i[a] ($M_\odot$)	$t_{\rm cool}+t_{\rm MS}$ (Gyr)	$\log \tau_D$ (yr)	References
0208+396	G74-7	0.60	7310	1.4	17	2.1	3.2	3.78	1, 2
0243−026	G75-39	0.70	6820	2.3	21	3.2	2.8	3.39	1, 2
0245+541	G174-14	0.76	5280	6.9	10	4.6	7.2	4.47	1, 2
1257+278	G149-28	0.58	8540	0.9	34	1.7	3.3	3.26	1, 2
1620−391	CD −38 10980	0.66	24406	0.1	12	3.1	0.7	...	3, 4

[a] See eq. (1) for the calculation of M_i and the WD's total ages.

REFERENCES.— (1) Bergeron et al. 2001; (2) Koester & Wilken 2006; (3) Bragaglia et al. 1995; (4) VizieR Online Data Catalog, 1238 (W. F. van Altena, J. T. Lee, & E. D. Hoffleit, 2001).

clouds are the result of planet formation, so the long-term evolution of planetary systems and their interaction with these comet clouds needs to be investigated (Tremaine 1993).

The loss of a star's outer envelope during post-main-sequence evolution specifically affects the stability of planetary systems, and can rescue the scenario proposed by Alcock et al. (1986). The Hill stability criterion against close approaches for two comparable mass planets qualitatively describes what happens to a planetary system. The stability criterion in this case is $\Delta_c = (a_1 - a_2)/a_1 = 3\mu^{1/3}$, where a is the semimajor axis, μ is the mass ratio of the planets to the host star, and Δ_c represents the critical separation at which the two planets become unstable to close approaches (Hill 1886; Gladman 1993). During adiabatic mass loss, companions expand their orbits in a homologous way, increasing their orbital semimajor axes by a factor M_i/M_f (Jeans 1924). The critical separation grows as the relative separation of the two planets stays the same, resulting in marginally stable systems being tipped over the edge of stability. This instability can lead to orbital rearrangements, the ejection of one planet, and collisions (Ford et al. 2001). These three events dramatically change the dynamical state of the planetary system. A fraction of unstable systems will perturb a surviving Oort Cloud or Kuiper Belt analog and send a shower of comets into the inner system, where they tidally disrupt, cause dust disks, and slowly settle onto the WD surface. This modification of the comet impact model can explain the accretion rates needed for the highest abundances of Ca observed and the presence of infrared excesses around WDs (Debes & Sigurdsson 2002).

The model of Debes & Sigurdsson (2002) can be extended to asteroidal material closer to the star. As the central star's mass changes, the basic resonances associated with any planets will change and bring fresh material into unstable orbits. The amount of pollution will depend on the different timescales for comets and asteroids to be perturbed toward the white dwarf as well as the ratio of objects in either asteroidal or cometary orbits. Asteroids should be perturbed relatively quickly, on timescales of 10^8 yr, while comets can take up to an order of magnitude longer to be perturbed. Without a more detailed model, however, it is hard to say which population is responsible for DAZ pollution.

Nine DAZs have already been searched for substellar companions at intermediate orbital separations (10 AU $< a <$ 50–100 AU) with NICMOS high-contrast imaging and AO imaging (Kuchner et al. 1998; Debes et al. 2005a, 2005b, 2006). No planets >10 $M_{\rm J}$ were detected for four, and no brown dwarfs >29 $M_{\rm J}$ were detected for the other five. In addition, no unresolved companions were detected down to substellar limits, following a general finding for a dearth of substellar objects around white dwarfs (Farihi & Christopher 2004; Dobbie et al. 2005; Farihi et al. 2005).

With the launch of *Spitzer* an unprecedented sensitivity is now possible to further constrain the presence of companions in close orbits, as well as the presence of dusty disks. A large interest in infrared excesses around white dwarfs in general is evidenced by the many surveys of white dwarfs with *Spitzer* (Hansen et al. 2006; Kilic et al. 2006b; Mullally et al. 2007; von Hippel et al. 2007; Jura et al. 2007a, 2007b).

In this paper we present results of our search of four nearby DAZs and a DA with circumstellar absorption that have no known excesses for companions and circumstellar disks. In § 2 we detail our *Spitzer* IRAC photometry and results, while in § 3 we present second-epoch NICMOS images of WD 1620−391 to look for common proper motion companions to the white dwarf. Finally, in § 4 we present our conclusions.

2. *SPITZER* PHOTOMETRY

2.1. *Observations*

Table 1 shows our target DAZs, complete with known $T_{\rm eff}$, log g, distances, and ages. Cooling ages were taken from the literature, and initial masses and main-sequence lifetimes were calculated by the equations of Wood (1992):

$$M_i = 10.4 \ln \frac{M_{\rm WD}}{0.49\ M_\odot}, \quad (1)$$

$$t_{\rm MS} = 10 M_i (M_\odot)^{-2.5}\ {\rm Gyr}. \quad (2)$$

Each target was observed with the four IRAC channels, with nominal wavelengths of ∼3.6, 4.5, 5.8, and 8.0 μm (Fazio et al. 2004). The observations were carried out in the mapping mode, with 30 random point dithers for each pair of channels. At each dither point the camera integrated for 100 s, for a total of 3000 s in each band. The exception to this was WD 1620−391, which is a much brighter source. The images had exposure times of 30 s per dither, with 75 dithers for a total integration of 2250 s. Table 2 summarizes our observations.

In order to obtain *Spitzer* IRAC photometry with an accuracy of ∼3%, we followed the prescription laid out in Reach et al. (2005a). We took the BCD files from the latest *Spitzer* pipeline calibrations for each target (S14.0) and created a final, mosaicked image using the MOPEX package (Makovoz & Marleau 2005). Some caution for point-source photometry with IRAC is warranted. Post-BCD pipeline calibrated mosaics are not of a high enough fidelity for accurate photometry of stellar point sources. We routinely found that PBCD images returned photometry systematically 2%–4% higher than when we used MOPEX. We performed overlap correction with a default overlap correction name-list, and mosaicking with the default name list given in the IRAC data handbook. For brighter point sources, the outlier rejection schemes of MOPEX can spuriously reject good pixels as cosmic rays due to photon noise larger than the background variation. A typical

TABLE 2
OBSERVATIONS

WD	AOR Key	Exposure Time (s)	Dither Points	Date	Start Time (UT)
0208+396	11389184	100	30	2005 Jan 17	20 35 48
0243−026	11389440	100	30	2005 Jan 16	15 44 34
0245+541	11389696	100	30	2005 Feb 19	03 34 52
1257+278	11389952	100	30	2005 Jun 13	03 18 19
1620−391	11390208	30	75	2005 Mar 30	10 12 15

symptom of this is a coverage map file that shows that many images were thrown out at the position of the target source. We experienced good results by choosing an UPPER_ and LOWER_THRESHOLD parameter of 15 for the MOSAICIN module, as well as using the keyword REFINE_OUTLIER to ensure bright sources were treated with a threshold closer to 20. The thresholds refer to the number of σ above the mean background. As a final check we visually inspected the resulting coverage maps to ensure that most images were used by the mosaicking program.

Since each of our images had several dither positions, we did not make any array-location or pixel phase corrections. We estimate that these effects are at the level of 1% and not a significant error source, but we include them in our total error. We performed aperture photometry with a 3 pixel radius ($\sim$3.6″), and used a 4 pixel wide annulus starting just outside the source aperture for background subtraction, to ensure as accurate an estimate of the background as possible. Aperture corrections appropriate for this size source radius and background annulus were applied, as well as calibration factors, flux conversions, and a color correction in each band assuming a ν^2 spectral slope, as mentioned in Reach et al. (2005a). The consistency of both aperture corrections and the photometry with different sized apertures was checked by recalculating the photometry with 5 pixel radius apertures with background annuli with 5 pixel radii starting just outside the source aperture, and 3 pixel source apertures with 10 pixel wide annuli starting at a radius of 10 pixels. We avoided a 2 pixel source aperture, as that appeared to consistently give photometry lower by $\sim$2%–5%. For channels 1 and 2, differences between the three choices were never more than 1%, except in the case of WD 0245+541, which has several nearby sources within 4–10 pixels. Channels 3 and 4 often had larger changes for the 5 pixel radius aperture, up to $\sim$10% but typically closer to 2%. We attribute these systematic changes primarily to residual structure in the background and to coincident sources. Both of these sources of systematic error are lessened by the small aperture and small background annulus. We estimate that on average there is a 1% error from systematic uncertainties in aperture photometry based on our specific choice of aperture and background annulus.

No obvious interstellar cirrus was noted for any of our targets in the 8 μm channel. Figures 1–3 show point-spread function (PSF)–subtracted NICMOS images of the DAZs from Debes et al. (2005b) with contours from the final IRAC channel 2 images overlaid. The contour lines correspond to 0.1%, 1%, and 10% of the total measured flux to demonstrate the absence of contaminating objects in the source and background photometric apertures. The target WD in each image is located at the point (0,0), and appears as a speckled area, since it is behind the coronagraph and the residual PSF has been subtracted off.

For the observations of WD 0208+396, the IRAC detector was struck by a large number of solar protons, degrading the images

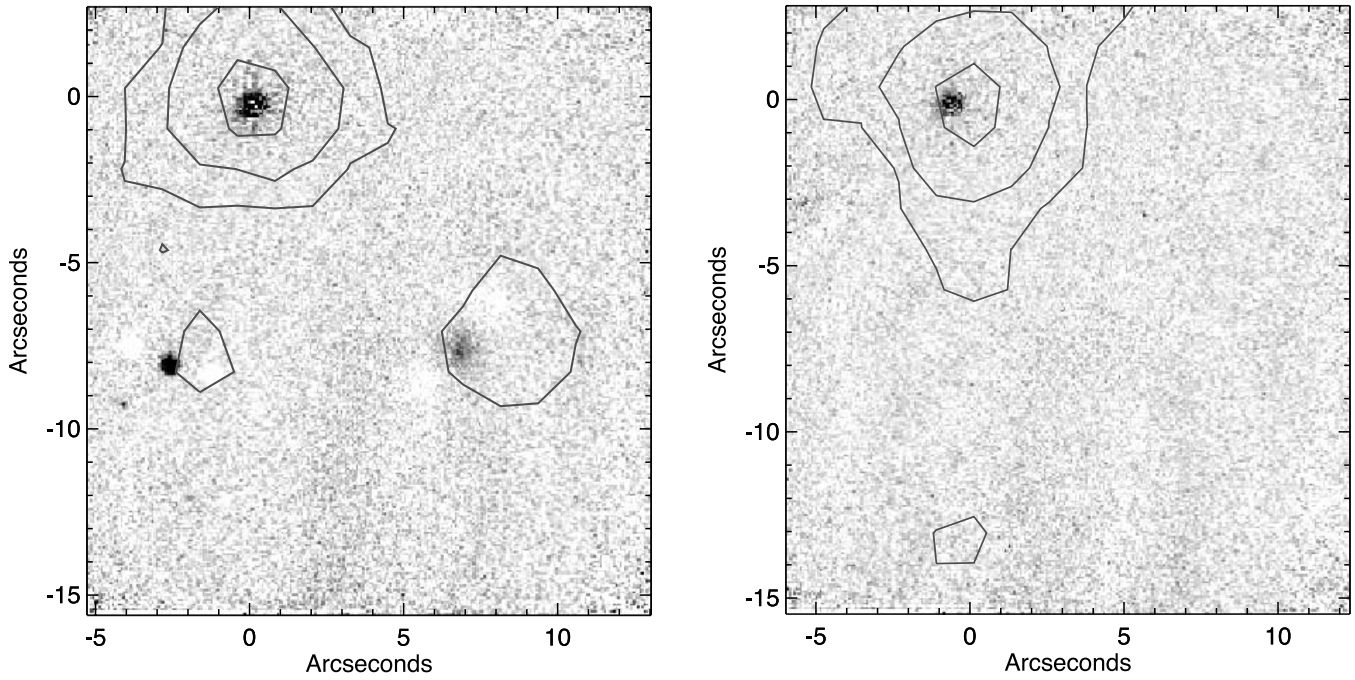

FIG. 1.—NICMOS F110W images of WD 0208+396 (*left*) and WD 0243−026 (*right*). The contours are from IRAC channel 2 images where the levels correspond to 0.1%, 1%, and 10% of the total observed flux from the white dwarf. [*See the electronic edition of the Journal for a color version of this figure.*]

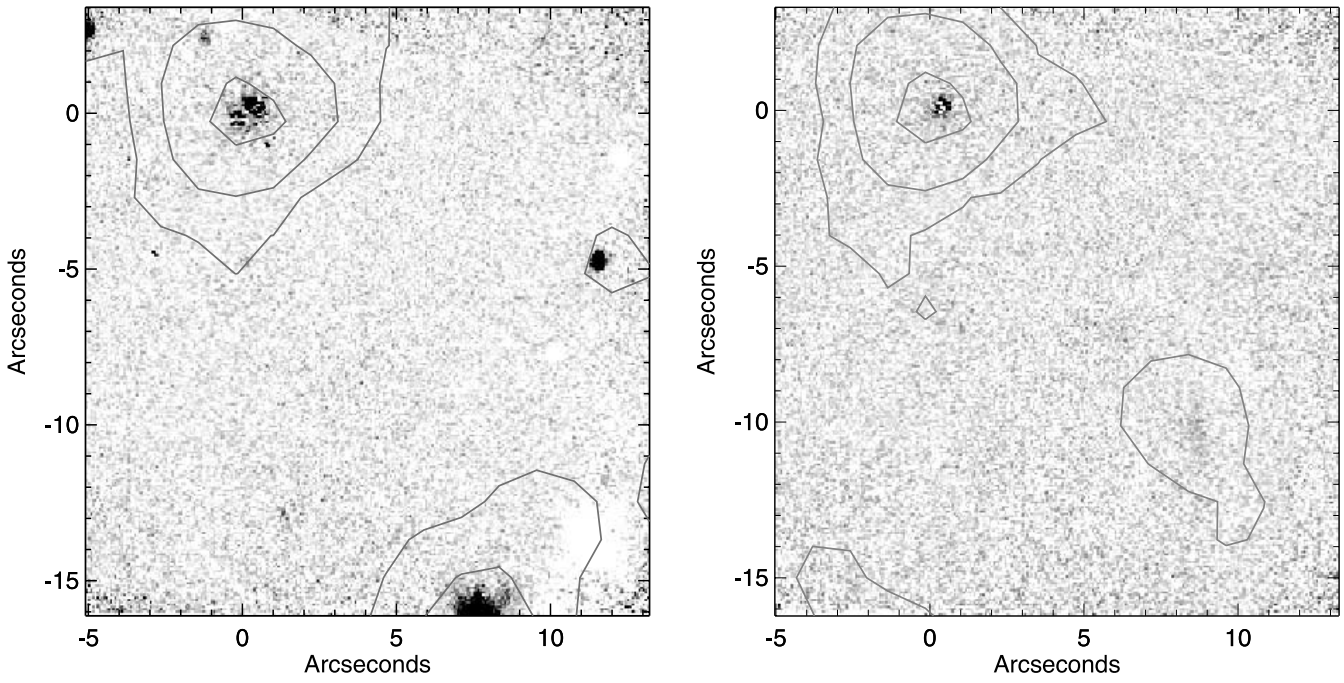

FIG. 2.—NICMOS F110W images of WD 0245+541 (*left*) and WD 1257+271 (*right*). The contours are from IRAC channel 2 images where the levels correspond to 0.1%, 1%, and 10% of the total observed flux from the white dwarf. [*See the electronic edition of the Journal for a color version of this figure*.]

with cosmic-ray hits. The looser constraints on outlier rejection can give higher counts at the level of 10%. These hits were worse for the 5.8 μm channel but we used a more stringent threshold for the MOPEX outlier routines of 3 for channels 3 and 4 instead of 15. Inspection of the coverage maps for the channels shows that most of the images could still be used, with the most images being rejected for the 5.8 μm channel. We verified that we got consistent photometry by visually inspecting individual BCD images and combining only the files without obvious cosmic-ray strikes.

The estimated photometric errors for each channel are quite small due to the large signal-to-noise ratio achieved. In addition to the standard errors in photometry, we added a 3.3% factor to account for the overall uncertainty in the flux calibrations quoted by Reach et al. (2005a), as well as the contributions from uncertainties mentioned above.

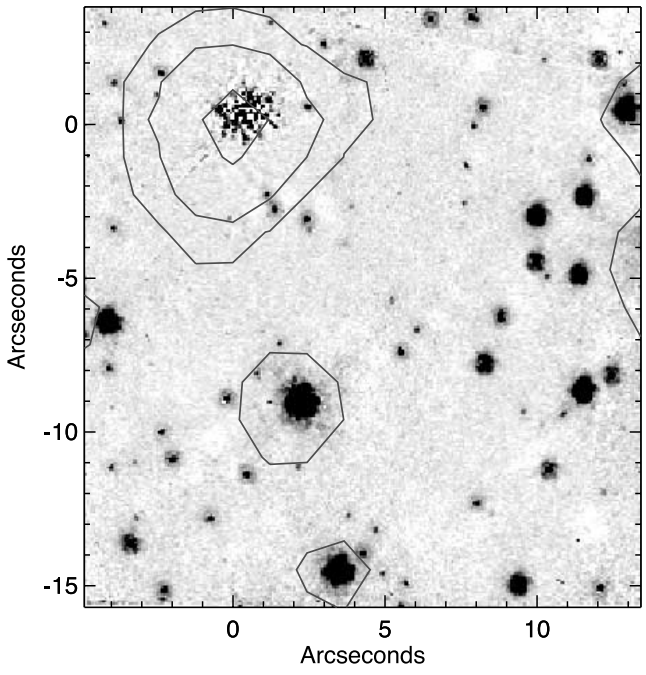

FIG. 3.—NICMOS F160W image of WD 1620−391. The contours are from IRAC channel 2 images where the levels correspond to 0.1%, 1%, and 10% of the total observed flux from the white dwarf. [*See the electronic edition of the Journal for a color version of this figure*.]

2.2. *Comparison of Photometry to WD Models*

In order to detect a bona fide excess, one must compare the observed flux with an expected flux. We compared our observations with models of Bergeron et al. (1995) as well as the *BVRIJHK* photometry of Bergeron et al. (2001) for four of the five targets. WD 1620−391 was not part of Bergeron et al. (2001)'s survey, and so we used a combination of USNOB, *Hipparcos*, and 2MASS photometry. Fluxes in the mid-infrared were kindly provided (P. E. Tremblay 2006, private communication), using updated models from Tremblay & Bergeron (2007) and without any knowledge of the measured mid-IR fluxes. We further normalized these flux densities to a median of the visible and near-IR flux densities to account for any slight offsets between the observed data and the models. This approach differs from previous work reported, where blackbody extrapolations of the WDs' K flux density were compared with our *Spitzer* data (Debes & Sigurdsson 2007).

For the level of photometric accuracy we have achieved, white dwarfs with an effective temperature of $\sim$5000−7000 K depart from true blackbodies, mainly due to H^- bound-free and free-free opacity, with the free-free opacity being most important for the near- and mid-infrared (P. E. Tremblay 2006, private communication). Free-free absorption can be calculated precisely at long wavelengths and is incorporated in WD models (see, e.g., John 1988).

Figure 4 shows a representative comparison between the model fluxes and the measured fluxes for WD 0208+396, as well as the residuals. The full list of predicted and observed IRAC fluxes for all of our targets is in Table 3, while Figures 5 and 6 show the

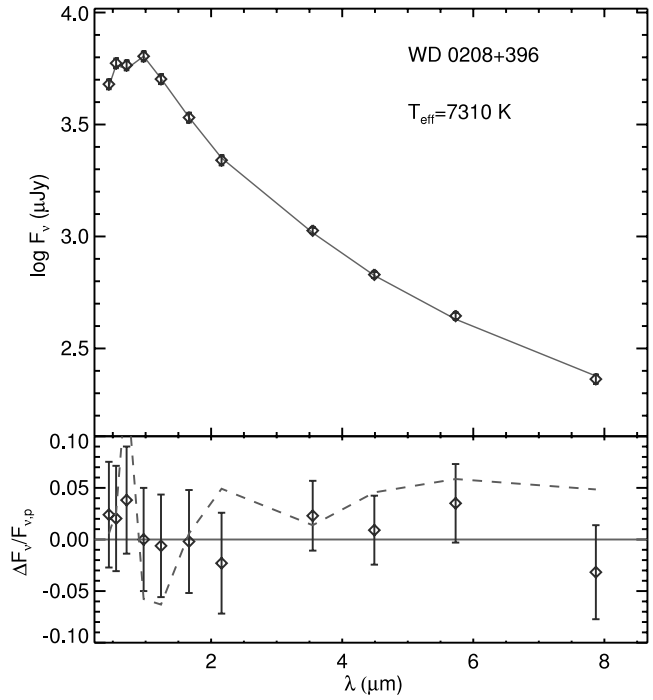

FIG. 4.—Comparison of observed fluxes for WD 0208+396 (*diamonds*) and predicted fluxes (*solid line*) based on the models of Bergeron et al. (2001). The bottom panel shows a close-up of the residuals in the IRAC channels, as well as the differences compared to a pure blackbody SED (*dashed line*). [*See the electronic edition of the Journal for a color version of this figure*.]

spectral energy distributions of the remaining targets. We required that a significant excess (deficit) be more than 3 times the photometric error above (below) the calculated model flux in at least one channel. We find that for the exception of WD 1257+278, the model fluxes and photometry agree to within $1-2\ \sigma$.

Figure 6 shows the SED of WD 1257+278 compared to the model. There is exactly a $3\ \sigma$ deficit in the 4.5 band, to a depth of 10%. The mosaic coverage maps show no images being thrown out where the photometric aperture is located. A slight mismatch between the model effective temperature and the true effective temperature could present an artificial deficit or excess, but the errors in the derived effective temperature are on the order of $\sim$2%, which would correspond to errors in the predicted fluxes of 3%–4%, much less than the observed deficit (P. E. Tremblay 2006, private communication). Despite matching our criteria for selection as a significant deficit, we believe it is tentative at best, based on a detailed analysis of the match between our photometry and the models.

Because of the deficit with WD 1257+278 we wished to get an empirical sense of how well the data matched the predicted model fluxes. To that end, we took the standard deviation of $\Delta F_\nu/F_{\nu,p}$ in all the channels, where ΔF_ν is the difference between the observed flux density and the predicted flux density ($F_{\nu,p}$), as well as the mean $\Delta F_\nu/F_{\nu,p}$ for each channel. We find that the standard deviation of the sample is $\sim$3.7%, while the mean for each channel is -1%, -5%, 0.09%, and -3%. These results indicate that the predicted fluxes match the observed fluxes to within the absolute calibration errors we assume. We note that the 4.5 μm channel appears to have a barely marginal ($\sim 1.4\ \sigma$) mean deficit, with four of the five targets possessing $\sim$5% or greater deficits, WD 1257+278 being one of these objects. WD 0208$-$396 is the only object with no deficit at 4.5 μm.

As another test, we divided the IRAC photometry of our target DAZs by WD 1620$-$391, the brightest WD in our sample with the highest signal-to-noise ratio. In this case we are limited by photon noise and the stability of the IRAC detectors, which is on the level of $\sim$2%. We compared the relative photometry of WD 1620$-$391 and WD 1257+278 to the model fluxes in Figure 7. Within the estimated errors, the observed flux ratios match the expected ratios. We repeated this test with the other white dwarfs and found similar agreement. The consistency of the flux ratios suggests that the depression of flux at 4.5 μm may be due to a systematic error in the aperture correction, color correction, or calibration factors for that channel.

Observed deficits for a white dwarf may be evidence for circumstellar material raining down on its surface. If such a situation were confirmed at 4.5 or 8 μm, we predict that non-LTE absorption by SiO gas may be present, with possibly some contribution from CO. Absorption due to fundamental and overtone rotational-vibrational bands of SiO and CO in late type stars is well known (Cohen et al. 1992). The dissociation temperature of SiO and CO are high enough that these species could persist at the temperatures of cooler white dwarfs.

The absorption could be boosted if SiO is formed above the white dwarf photosphere through photodissociation of SiO_2 (and any CO present is similarly formed through photodissociation of carbonates) from refractory dust which sublimates as it is brought down to the white dwarf surface through photon drag. The resulting SiO is formed at low densities just above the photosphere, and is far from local thermodynamic equilibrium, with much larger absorption strengths than inferred from photospheric LTE. This absorption would show up most strongly around 4–5 μm and $\sim$8–10 μm where SiO has fundamental and first overtone bands at 8.0 and 4.1 μm, respectively. CO would show up primarily in the second channel with its fundamental band at 4.7 μm (Cohen et al. 1992). The details of this scenario need to be studied further to determine the feasibility of observing absorption due to SiO or CO gas.

2.3. *Limits to Companions*

For IRAC, very cool substellar objects can be detected as excesses, especially due to a "bump" of flux for brown dwarfs and planets at $\sim$4.5 μm. While theoretical models predict the 4.5 μm flux to be large, observations of cool brown dwarfs suggest that the spectral models overestimate this flux by a factor of $\sim$2 (Golimowski et al. 2004; Patten et al. 2006).

TABLE 3
PREDICTED AND OBSERVED FLUXES IN μJy

WD	$[3.6]_p$	$[3.6]_o$	$[4.5]_p$	$[4.5]_o$	$[5.8]_p$	$[5.8]_o$	$[8.0]_p$	$[8.0]_o$
0208+396	1039	1063 ± 35	669	676 ± 22	426	442 ± 16	238	231 ± 11
0243−026	472	479 ± 16	307	294 ± 10	196	198 ± 7	110	102 ± 5
0245+541	1333	1305 ± 43	894	848 ± 28	587	583 ± 20	336	332 ± 12
1257+278	300	290 ± 10	192	175 ± 6	122	124 ± 5	68	71 ± 4
1620−391	5100	5162 ± 170	3204	3050 ± 90	2006	2008 ± 67	1097	1050 ± 35

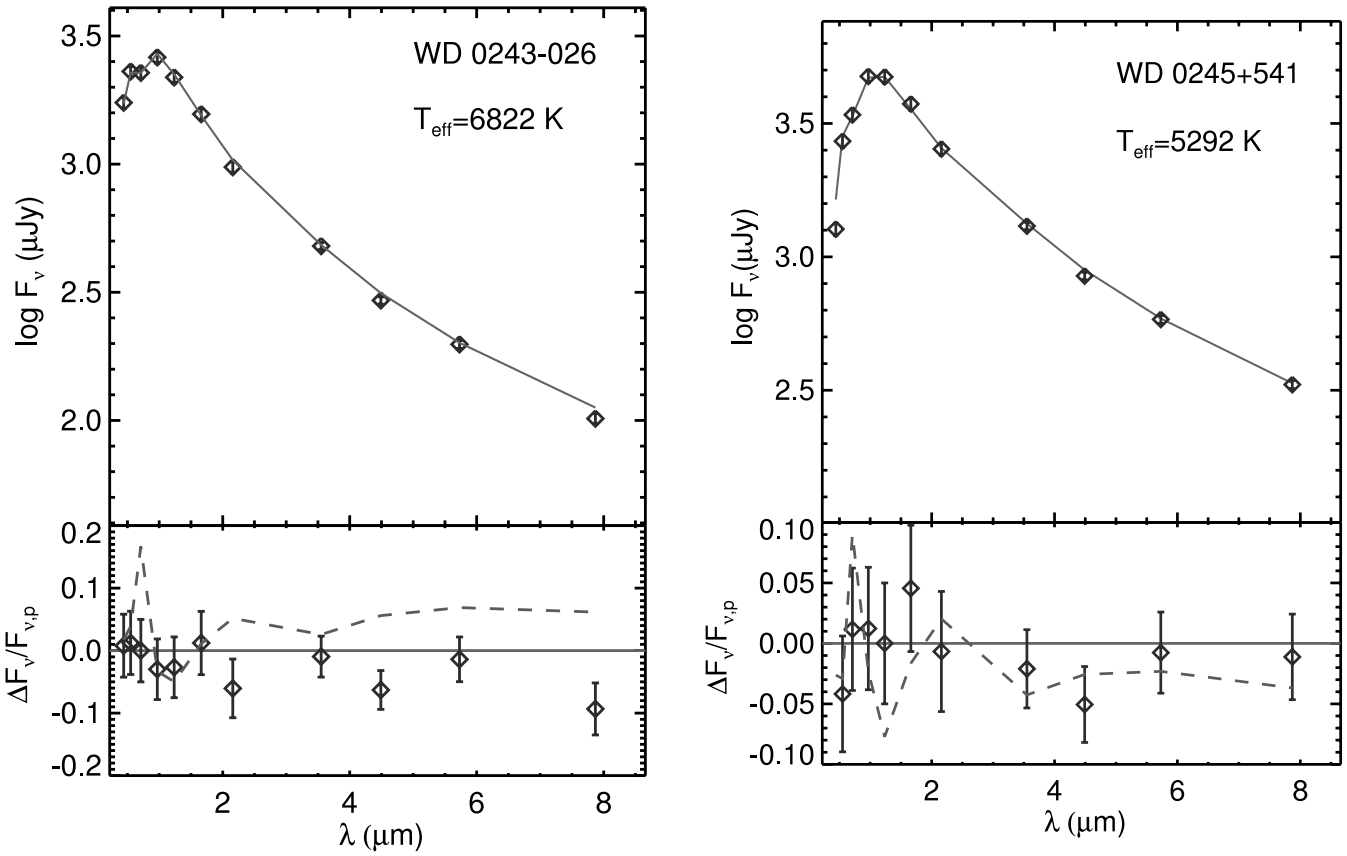

FIG. 5.—Same as Fig. 4, but for WD 0243−026 (*left*) and WD 0245+541 (*right*). [*See the electronic edition of the Journal for a color version of this figure.*]

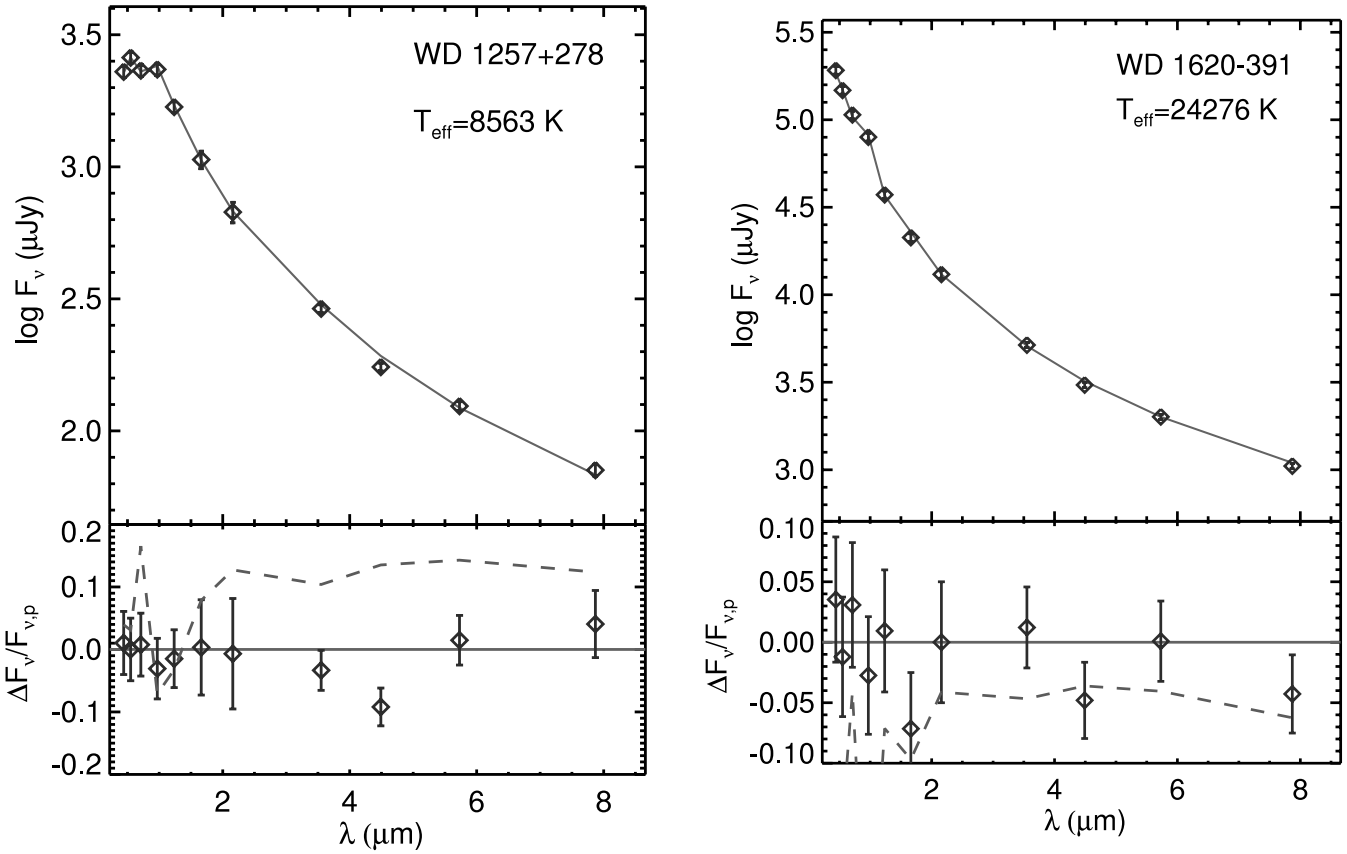

FIG. 6.—Same as Fig. 4, but for WD 1257+278 (*left*) and WD 1620−391 (*right*). [*See the electronic edition of the Journal for a color version of this figure.*]

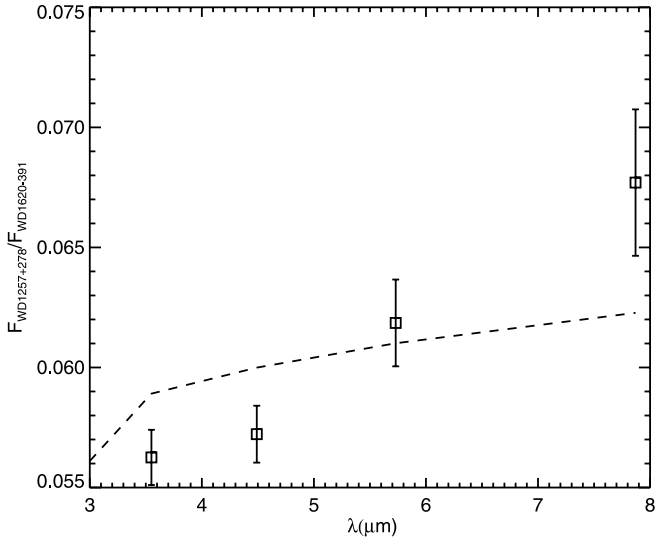

FIG. 7.—Comparison between the measured flux ratio of WD 1257+278 to WD 1620−391 (*squares*) and that predicted by white dwarf models (*dashed line*). WD 1257+278 shows a significant deficit in its absolute photometry which is not reproduced relative to WD 1620−391.

In order to place upper limits on the types of unresolved companions present around our targets, we compared predicted IRAC fluxes for cool brown dwarfs and planets by convolving the IRAC filters with the models of Burrows et al. (2003) appropriate for the particular age of each target DAZ and its distance. For the 4.5 μm channel we assumed that the resultant flux was a factor of 2 smaller than predicted. We then compared our 4.5 μm 3 σ limits to those models in order to determine a mass limit. These results are presented in Table 4. In all cases we improve the unresolved companion limits to these objects over Debes et al. (2005b) by a factor of 2–4. For WD 0243−026 and WD 1620−391 we rule all companions >14 M_J objects for separations <76 and 46 AU, respectively.

2.4. *Limits to Dusty Disks*

We can determine limits to two types of dusty disks, either geometrically flat, optically thick disks, such as that modeled for G29-38 or GD 362, or diffuse, optically thin disks. Both GD 362 and G29-38 can be well modeled by disks not unlike Saturn's rings, within the tidal radius of the white dwarf with an interior edge at the dust sublimation radius (Jura 2003; Becklin et al. 2005; Jura et al. 2007b; von Hippel et al. 2007).

2.4.1. *Optically Thick Disks*

If we assume an optically thick disk, the emission of the grains can be modeled following Adams et al. (1987):

$$F_\nu = \frac{2\pi \cos i}{d^2} \int_{R_{\rm in}}^{R_{\rm out}} B_\nu(T) r\, dr, \quad (3)$$

with T as a function of R:

$$T = \left(\frac{2}{3\pi}\right)^{1/4} \left(\frac{R_*}{r}\right)^{3/4} T_*. \quad (4)$$

This assumes that the inner radius corresponds to a dust sublimation radius of 1200 K. In Table 4 we show the upper limits to i based on our lack of 3 σ detections in our 8.0 μm channel data. In most cases, excess emission would have been significantly detected at shorter wavelengths as well. If this type of disk is present around these DAZs, the inner edge of the disks must be at 0.4 $R_\odot$, or all of them are close to edge-on. We can quantify the probability of observing five systems with inclinations determined by our upper limits out of a random sample of disk inclinations. For any one disk, this is $\sim 1 - \cos i$, and for all five targets the probability is negligible. Most optically thick dust disks observed seem to have exterior radii of <0.6 $R_\odot$ (von Hippel et al. 2007).

TABLE 4
EXCESS LIMITS

WD	Companion Limit (M_J)	i[a] (deg)	$R_{\rm in}$[b] ($R_\odot$)	Dust Mass[c] (g)
0208+396	20	2.9	0.7	2×10^{20}
0243−026	14	4.7	0.5	2×10^{20}
0245+541	20	1.6	0.4	1×10^{20}
1257+278	20	10.7	0.7	8×10^{20}
1620−391	13	0.1	5.0	...

[a] Upper inclination limit for optically thick disk to avoid detection.
[b] Lower limit for inner radius of optically thick disk.
[c] Upper mass limit of dust for optically thin disk.

Given the 10^3–10^4 yr settling timescales (t_D; see Table 1) for our targets, the lack of a disk does not necessarily imply that the DAZs cannot accrete material in this manner. As Hansen et al. (2006) has pointed out, the timescale for removal of dust grains within the tidal disruption radius of a white dwarf due to Poynting-Robertson drag is short:

$$T_{\rm PR} = \left(\frac{s}{1\ \mu{\rm m}}\right)\left(\frac{\rho_s}{3\ {\rm g\ cm^{-3}}}\right)\left(\frac{r}{10^{10}\ {\rm cm}}\right)^2\left(\frac{L_*}{10^{-3}\ L_\odot}\right)\ {\rm yr}, \quad (5)$$

where s and ρ_s are the average grain size and density respectively, and r is the distance from the star, ranging from $\sim 10^{10}$ to 10^{11} cm. If an incoming comet or asteroid is disrupted and all of the material is removed before another arrives, then for some fraction of the time a DAZ will have this type of disk and at other times it will not, while still retaining a detectable metal-line signature. The metal line will remain detectable as long as the metal settling time is roughly longer than the time to the next replenishing collision. Cooler dust from collisions may still be detectable at longer wavelengths, or may slowly drift inwards from further away. Using equation (5), one can determine the rough orbital separation from which dust would spiral in over 1 Gyr, or a typical cooling time for a white dwarf. Assuming the typical values in equation (5), dust could spiral in from as far as $\sim$20 AU.

2.4.2. *Optically Thin Disks*

If we expect an optically thin disk, we see the emission from every emitter. If one assumes a particular size (and therefore a particular mass) per emitter and the number of emitters per unit area, one can determine the total mass in an optically thin dust disk based on the observed flux. We focus in particular on the limit to dust between the tidal radius of the white dwarf and the dust sublimation radius, since this region is of most interest for explaining DAZ metal accretion.

For the sake of simplicity, we assume that a constant number density of 1 μm dust particles reside in a flat optically thin disk between the dust sublimation radius $R_{\rm sub}$ and the approximate tidal disruption radius, $R_{\rm tidal} \sim (\bar{\rho}_{\rm WD}/\rho_{\rm obj})^{1/3} R_*$ of the DAZ, assuming a

$\rho_{\rm obj} = 3$ g cm^{-3} for the parent bodies to the dust. In this case the flux is given by a modification of equation (3):

$$F_\nu = \frac{2\pi s^2 \cos i}{d^2} \int_{R_{\rm sub}}^{R_{\rm tidal}} n(r) B_\nu(T) r\, dr, \qquad (6)$$

where we have used the models of Laor & Draine (1993) to calculate the spherical 1 μm grain temperature of each dust particle given each DAZs luminosity (Bergeron et al. 2001; Bragaglia et al. 1995). For each WD we normalize $n(r)$ such that the resulting dust disk spectrum returns the 3 σ flux limit when convolved with the IRAC 8 μm channel filter response. Table 4 shows the resulting upper limits for dust disk mass. For WD 1620−391, the radius at which dust sublimates exceeds the tidal disruption radius, and so we expect no dust to be present in this region. Similarly, hot white dwarfs would not have dusty disks around them like G29-38 or GD 362. They may have gaseous disks around them, as evidenced by the discovery of a gaseous, metal-rich disk around a hot DA white dwarf (Gänsicke et al. 2006).

If there are dust disks, then dust accretion could conceivably occur for longer then the DAZ atmospheric settling times in our sample. However, the PR drag timescale at the tidal disruption radius for each DAZ is $\lesssim M_{\rm disk}/\dot{M}$. This implies that accretion is not driven by PR drag of a present disk.

3. NICMOS IMAGING

NICMOS coronagraphic images of these five white dwarfs were presented in Debes et al. (2005b) with accompanying limits to companions at 1.1 μm, as well as 1.6 μm for WD 1620−391. High spatial resolution NIR images are particularly useful for discriminating against potential sources of background contamination which could bias the mid-IR photometry to spurious excesses, given the IRAC camera's spatial resolution of 1.2″ pixel^{-1}. While it may be rare to find coincident sources that may contaminate the photometry of the target, two of the five targets have visual companions within 4″ of the target star.

WD 1620−391, one of the targets with a large number of visual companions, is close to the Galactic plane. This interesting object is not technically a DAZ. It is a DA with no optical metal absorption lines that is a large separation common proper motion companion to a planet-bearing star (Mayor et al. 2004). In the UV it possesses metallic circumstellar absorption lines (Holberg et al. 1995; Wolff et al. 2001). The planet-bearing star is separated by 5.75′ (4451 AU), and is well off the field of view for NICMOS. Even expecting a large number of coincident sources due to its Galactic latitude, it possessed an overdensity over that expected (Debes et al. 2005b). Motivated by this overdensity, a second epoch image of WD 1620−391 was obtained in 2006 March, 2 yr after the first image was taken to search for any common proper motion companions. The new image was reduced following the basic prescription laid out in Debes et al. (2005b), where the white dwarf was imaged at two separate spacecraft roll orientations and each roll image was subtracted from the other and combined to produce a high-contrast final image. The other objects in the field were masked out in the image that was used as a PSF reference, since the field of view was moderately crowded and subtraction residuals would hamper the detection of faint sources.

We aligned both epochs on the pixel position of WD 1620−391 and rotated the images so that north was in the positive vertical direction of the images, using pixel centers and orientations as header keywords from the STScI pipeline. We then shifted the second-epoch image by the measured proper motion of WD 1620−391 of 97.49 ± 3.28 mas yr^{-1} ($\mu \cos \delta = 75.52$ mas yr^{-1}) in right ascension and 0.05 ± 1.74 mas yr^{-1} in declination (Perryman et al. 1997) to align the shifted background stars. We measured the centroids of ∼70 observed objects common in both fields using the IDL ASTROLIB routine `gcntrd` and measured the difference in centroid position from one epoch to another. With this procedure, any object comoving with WD 1620−391 would have a position shift of 2.58 NICMOS pixels, or 0.19″.

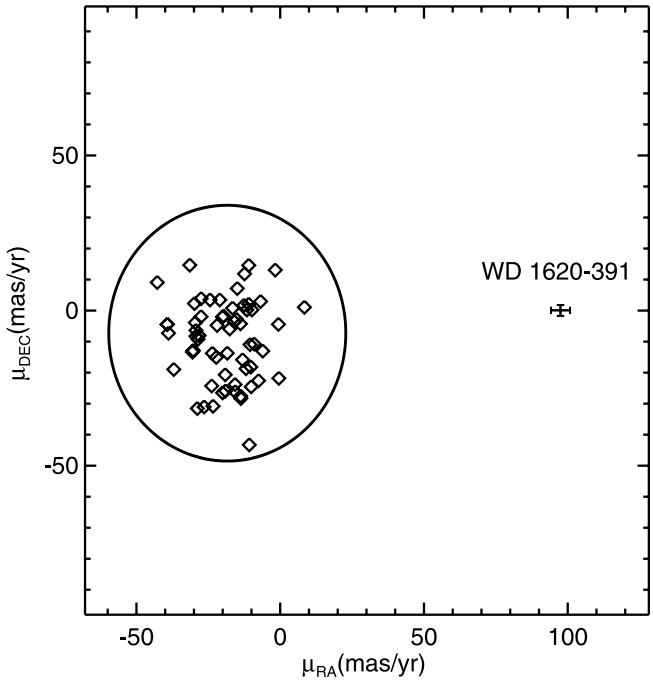

FIG. 8.—Measured proper motion in declination vs. proper motion in right ascension for observed sources close to WD 1620−391. The circle represents the 3 σ scatter of the observed objects, while the barred cross denotes where an object comoving with WD 1620−391 would lie.

Figure 8 shows the resulting differences between the measured centroids in the two NICMOS image epochs. The solid circle represents the 3 σ limit as empirically measured by the entire sample of observed sources in the field, with 1 σ being 14 mas yr^{-1} and median proper motions of the sample of −17 and −8 mas yr^{-1}. There is a slight offset in the median change in right ascension of the group of sources from the expected zero value, although it is a ∼1 σ difference in right ascension. This could be because of a bulk proper motion of the background sources, since WD 1620−391 is at a low Galactic latitude, or a subpixel mismatch between the reported pixel centers of WD 1620−391. The magnitude of centroiding errors on *Hubble Space Telescope* acquisitions, however, is closer to 7 mas and is smaller than the offset seen here. In any case, there appear to be no comoving sources, thus completely ruling out any companions down to 6 $M_{\rm J}$ at separations >13 AU (Debes et al. 2005b).

4. CONCLUSIONS

We can place stringent limits on the types of disks and unresolved companions present for all of our targets. For two of our targets, only planetary-mass objects ($M < 14\,M_{\rm J}$) can be present at all separations, and for the rest only very low mass brown dwarfs ($M < 20\,M_{\rm J}$) can be present at separations <1″ or orbital separations of between 13 and 35 AU.

The explanation that all apparently single DAZs can be caused by the winds of unseen companions does not fit our results unless the companions are very low mass brown dwarfs or high-mass planets. One would expect to see large amounts of dust present if

tidally disrupted planetesimals or ISM accretion were the source of metals for DAZs. Our targets show no evidence of such dust down to $\sim 10^{20}$ g if there are optically thin disks present, and out to separations of $\sim 0.4\ R_{\odot}$ if there are optically thick disks present. We effectively rule out optically thick disks like those seen around G29-38 for our targets. We cannot rule out dust that is farther away from the white dwarf and consequently much cooler. Sensitive studies at longer wavelengths may yet detect dust around these white dwarfs.

Instead, optically thick dusty disks around DAZs seem to be somewhat rare with only five such known and no optically thin disks yet reported (Zuckerman & Becklin 1987; Farihi et al. 2005, 2006; Kilic et al. 2005, 2006a; Kilic & Redfield 2007). A lack of optically thick dust can be explained for cooler DAZs by infrequent encounters with large planetesimals that create short-lived disks that disappear quickly while still allowing detectable metal lines. For that reason dusty disks should primarily be around hotter DAs, whose shorter settling times require a quicker replenishment of dust and thus should have long-lived disks. DAs that are too hot vaporize material well before it is tidally disrupted. If the disks are instead optically thin, then weaker emission may be present, although currently undetectable. The upper limits for dust disk masses imply that for many DAZs the amount of material close to the white dwarf is sufficient to be detectable spectroscopically, but more difficult to detect in the mid-IR.

The authors would like to thank the anonymous referee for useful suggestions in improving this paper. We would like to thank Pierre Bergeron and Pier-Emmanuel Tremblay for helpful discussions on model white dwarf atmospheres and for graciously providing model flux densities. This work is based in part on observations made with the *Spitzer Space Telescope*, which is operated by the Jet Propulsion Laboratory, California Institute of Technology, under a contract with NASA. Support for this work was provided by NASA through an award issued by JPL/Caltech. Support for program 10560 was provided by NASA through a grant from the Space Telescope Science Institute, which is operated by the Association of Universities for Research in Astronomy, Inc., under NASA contract NAS5-26555.

REFERENCES

Aannestad, P. A., Kenyon, S. J., Hammond, G. L., & Sion, E. M. 1993, AJ, 105, 1033
Adams, F. C., Lada, C. J., & Shu, F. H. 1987, ApJ, 312, 788
Alcock, C., Fristrom, C. C., & Siegelman, R. 1986, ApJ, 302, 462
Althaus, L. G., & Benvenuto, O. G. 1998, MNRAS, 296, 206
Becklin, E. E., Farihi, J., Jura, M., Song, I., Weinberger, A. J., & Zuckerman, B. 2005, ApJ, 632, L119
Bergeron, P., Leggett, S. K., & Ruiz, M. T. 2001, ApJS, 133, 413
Bergeron, P., Wesemael, F., Lamontagne, R., Fontaine, G., Saffer, R. A., & Allard, N. F. 1995, ApJ, 449, 258
Bragaglia, A., Renzini, A., & Bergeron, P. 1995, ApJ, 443, 735
Burleigh, M. R., Clarke, F. J., & Hodgkin, S. T. 2002, MNRAS, 331, L41
Burrows, A., Sudarsky, D., & Lunine, J. I. 2003, ApJ, 596, 587
Cohen, M., Witteborn, F. C., Carbon, D. F., Augason, G., Wooden, D., Bregman, J., & Goorvitch, D. 1992, AJ, 104, 2045
Debes, J. H. 2006, ApJ, 652, 636
Debes, J. H., Ge, J., & Ftaclas, C. 2006, AJ, 131, 640
Debes, J. H., & Sigurdsson, S. 2002, ApJ, 572, 556
———. 2007, preprint (astro-ph/0703448)
Debes, J. H., Sigurdsson, S., & Woodgate, B. E. 2005a, ApJ, 633, 1168
———. 2005b, AJ, 130, 1221
Dobbie, P. D., Burleigh, M. R., Levan, A. J., Barstow, M. A., Napiwotzki, R., Holberg, J. B., Hubeny, I., & Howell, S. B. 2005, MNRAS, 357, 1049
Dupuis, J., Fontaine, G., Pelletier, C., & Wesemael, F. 1992, ApJS, 82, 505
———. 1993a, ApJS, 84, 73
Dupuis, J., Fontaine, G., & Wesemael, F. 1993b, ApJS, 87, 345
Farihi, J., Becklin, E. E., & Zuckerman, B. 2005, ApJS, 161, 394
Farihi, J., & Christopher, M. 2004, AJ, 128, 1868
Farihi, J., Zuckerman, B., Becklin, E. E., & Jura, M. 2006, preprint (astro-ph/0610101)
Fazio, G. G., et al. 2004, ApJS, 154, 10
Ford, E. B., Havlickova, M., & Rasio, F. A. 2001, Icarus, 150, 303
Friedrich, S., Zinnecker, H., Brandner, W., Correia, S., & McCaughrean, M. 2005, in ASP Conf. Ser. 334, 14th European Workshop on White Dwarfs, ed. D. Koester & S. Moehler (San Francisco: ASP), 431
Gänsicke, B. T., Marsh, T. R., Southworth, J., & Rebassa-Mansergas, A. 2006, Science, 314, 1908
Gladman, B. 1993, Icarus, 106, 247
Golimowski, D. A., et al. 2004, AJ, 127, 3516
Graham, J. R., Matthews, K., Neugebauer, G., & Soifer, B. T. 1990, ApJ, 357, 216
Hansen, B. M. S., Kulkarni, S., & Wiktorowicz, S. 2006, AJ, 131, 1106
Hill, G. W. 1886, Acta Math., 8, 1
Holberg, J. B., Bruhweiler, F. C., & Andersen, J. 1995, ApJ, 443, 753
Ignace, R. 2001, PASP, 113, 1227
Jeans, J. H. 1924, MNRAS, 85, 2
John, T. L. 1988, A&A, 193, 189
Jura, M. 2003, ApJ, 584, L91
Jura, M., Farihi, J., & Zuckerman, B. 2007a, ApJ, 663, 1285
Jura, M., Farihi, J., Zuckerman, B., & Becklin, E. E. 2007b, AJ, 133, 1927
Kilic, M., & Redfield, S. 2007, ApJ, 660, 641
Kilic, M., von Hippel, T., Leggett, S. K., & Winget, D. E. 2005, ApJ, 632, L115
———. 2006a, ApJ, 646, 474
Kilic, M., von Hippel, T., Mullally, F., Reach, W. T., Kuchner, M. J., Winget, D. E., & Burrows, A. 2006b, ApJ, 642, 1051
Koester, D., & Wilken, D. 2006, A&A, 453, 1051
Kuchner, M. J., Koresko, C. D., & Brown, M. E. 1998, ApJ, 508, L81
Laor, A., & Draine, B. T. 1993, ApJ, 402, 441
Makovoz, D., & Marleau, F. R. 2005, PASP, 117, 1113
Maxted, P. F. L., Napiwotzki, R., Dobbie, P. D., & Burleigh, M. R. 2006, Nature, 442, 543
Mayor, M., Udry, S., Naef, D., Pepe, F., Queloz, D., Santos, N. C., & Burnet, M. 2004, A&A, 415, 391
Mullally, F., Kilic, M., Reach, W. T., Kuchner, M. J., von Hippel, T., Burrows, A., & Winget, D. E. 2007, ApJS, 171, 206
Parriott, J., & Alcock, C. 1998, ApJ, 501, 357
Patten, B. M., et al. 2006, ApJ, 651, 502
Patterson, J., Zuckerman, B., Becklin, E. E., Tholen, D. J., & Hawarden, T. 1991, ApJ, 374, 330
Perryman, M. A. C., et al. 1997, A&A, 323, L49
Probst, R. G., & O'Connell, R. W. 1982, ApJ, 252, L69
Reach, W. T., Kuchner, M. J., von Hippel, T., Burrows, A., Mullally, F., Kilic, M., & Winget, D. E. 2005a, ApJ, 635, L161
Reach, W. T., et al. 2005b, PASP, 117, 978
Tremaine, S. 1993, in ASP Conf. Ser. 36, Planets Around Pulsars, ed. J. A. Phillips, S. E. Thorsett, & S. R. Kulkarni (San Francisco: ASP), 335
Tremblay, P., & Bergeron, P. 2007, ApJ, 657, 1013
von Hippel, T., Kuchner, M. J., Kilic, M., Mullally, F., & Reach, W. T. 2007, ApJ, 662, 544
Wolff, B., Kruk, J. W., Koester, D., Allard, N. F., Ferlet, R., & Vidal-Madjar, A. 2001, A&A, 373, 674
Wood, M. A. 1992, ApJ, 386, 539
Zuckerman, B., & Becklin, E. E. 1987, Nature, 330, 138
———. 1992, ApJ, 386, 260
Zuckerman, B., Koester, D., Reid, I. N., & Hünsch, M. 2003, ApJ, 596, 477
Zuckerman, B., & Reid, I. N. 1998, ApJ, 505, L143